Institute of Physics Publishing | Plasma Sources Science and Technology
Plasma Sources Sci. Technol. **15** (2006) 204–210 doi:10.1088/0963-0252/15/2/005

Properties of an atmospheric pressure radio-frequency argon and nitrogen plasma

M Moravej[1], X Yang[1], M Barankin[1], J Penelon[2], S E Babayan[2] and R F Hicks[1]

[1] Chemical Engineering Department, University of California, Los Angeles, CA 90095
[2] Surfx Technologies LLC, 3617 Hayden Ave., Culver City, CA 90232

E-mail: rhicks@ucla.edu

Received 4 August 2005, in final form 30 January 2006
Published 24 February 2006
Online at stacks.iop.org/PSST/15/204

Abstract
An atmospheric pressure capacitive discharge source has been developed that operates at power densities over 100 W cm^{-3}. The ground state nitrogen atom concentration was measured at the exit of the source by titration with NO, and it was found to reach a maximum of $3.0 \pm 0.8 \times 10^{17}$ cm^{-3} at 6.0 vol% N_2 in argon, 250 °C and 150 W cm^{-3}. This is equivalent to 2.3 vol% of N atoms in the afterglow. At these conditions, the electron density and temperature are estimated to be 3.1×10^{12} cm^{-3} and 1.2 eV. A plug-flow model of the plasma and afterglow was developed, and it was determined that the maximum N atom concentration achievable is limited by three body recombination.

1. Introduction

Nitrogen plasmas have numerous industrial applications. They are used in metal nitriding to improve surface hardness, wear and corrosion resistance and fatigue life [1, 2]. This method has been successfully applied to a large set of metals such as titanium, copper and gold, and to non-metals such as silicon and III–V compounds [2]. Nitrogen-containing plasmas are also used to treat the surfaces of organic polymers in order to change the wettability and promote adhesion [1, 2]. Furthermore, there are many applications of nitrogen plasmas in thin film deposition [1, 2]. All these processes may be accomplished by these discharges due to the high atomic nitrogen content produced by the plasma [2].

Industrial plasmas operate either at low pressures (<1 Torr) or at atmospheric pressure [3, 4]. Ambient pressure operation is advantageous over low pressure because it does not require vacuum systems and allows for continuous in-line processing. Thermal atmospheric pressure plasmas such as torches and arcs can be used for substrates that are not thermally sensitive or where contact time with the plasma can be kept short [1]. Recently, there has been great interest in non-equilibrium, atmospheric pressure plasmas. Examples of non-equilibrium atmospheric pressure plasmas include coronas [5, 6], dielectric barrier discharges (DBDs) [7–11], micro-hollow cathode discharges [12, 13] and noble-gas stabilized, capacitive discharges [14–19].

In this manuscript, we report on a new atmospheric pressure plasma that is struck inside a quartz tube using radio frequency power at 13.56 MHz and current densities up to 7.5 A cm^{-3}. The discharge physics indicate that it is capacitively coupled. This source produces a high concentration of ground state nitrogen atoms, about 2.0 vol% of the total gas and is well suited for materials processing.

2. Experimental methods

A schematic of the experimental apparatus is shown in figure 1(*a*). The plasma source consisted of a quartz tube, 2.0 mm inside diameter, which was mounted between two parallel aluminium electrodes. The length of the electrodes was varied between 2.5 and 12.5 cm to determine the effect of the residence time on the production of nitrogen atoms. One of the electrodes was supplied with radio frequency power at 13.56 MHz, while the other one was grounded. A tuned impedance probe (Advanced Energy RFZ 60) was inserted between the source and the matching network to determine the current–voltage characteristics of the discharge. To determine

0963-0252/06/020204+07$30.00 © 2006 IOP Publishing Ltd Printed in the UK

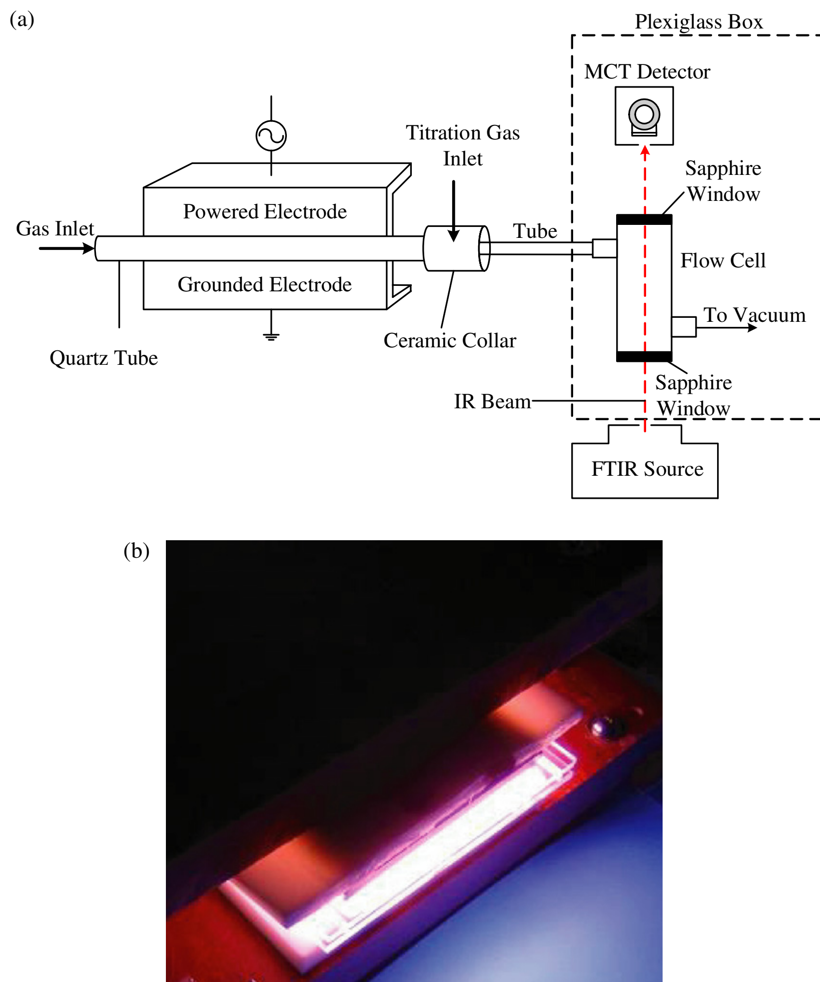

Figure 1. (*a*) Schematic of the experimental apparatus (not drawn to scale). (*b*) Picture of the plasma source with an area of $6.3 \times 6.3\,\mathrm{cm}^2$. (This figure is in colour only in the electronic version)

the time-dependent current and voltage waveforms, an IV probe was placed in the line between the impedance probe and the source. This probe was connected to an oscilloscope (Tektronix, TDS 224) that had a 5.0 ns time resolution.

A picture of a source operating on the same principles but with a larger area is shown in figure 1(*b*). Here the quartz tube has been replaced by two quartz sheets separated by a gap of 2.0 mm. Two parallel plate aluminium electrodes with an area of $6.3 \times 6.3\,\mathrm{cm}^2$ are mounted on the outside of the quartz sheets. The quartz plates are larger than the electrodes to prevent arcing. The plasma shown in the picture is a pure argon discharge operating at $50\,\mathrm{W\,cm^{-3}}$.

The gas temperature of the argon and nitrogen discharge was determined by optical emission spectroscopy (OES). The light was collected with a fibre optic cable that was attached to a monochromator (Instruments S.A., Triax 320). The monochromator was equipped with a $1200\,\mathrm{groove\,mm^{-1}}$ grating and a liquid nitrogen cooled CCD (Instruments S.A., CCD-3000). A slit width of 0.1 mm was used resulting in a spectral resolution of 0.23 nm. To measure the gas temperature, the rotational temperature of the (3,0) band of the N_2 first positive emission spectrum was fitted to a Boltzmann plot [20].

The concentration of the ground state nitrogen atoms was determined by titration with nitric oxide (NO), which produced nitrogen dioxide (NO_2) [15]. For these experiments, a ceramic collar was inserted on the end of the quartz tube [21]. This ceramic collar had a small opening, 0.5 cm downstream of the plasma, through which the NO was introduced. Another tube connected the gas effluent to an infrared flow cell that was pumped at the other end. A Fourier-transform infrared spectrometer (BioRad FTS-7) was used to monitor the titration process. The infrared beam passed into and out of the flow cell through KBr windows, and the beam path length was 20 cm. The light was collected with a mercury–cadmium–telluride (MCT) detector at a resolution of $1\,\mathrm{cm^{-1}}$ and by signal averaging 64 scans.

3. Results

3.1. Discharge physics

Current–voltage curves for the argon and 1.0 vol% nitrogen plasma are presented in figure 2. Different electrode/plasma lengths were examined ranging between 2.5 and 12.5 cm. The curves only show the regime beyond gas breakdown. Before the plasma was struck, the discharge followed a Townsend

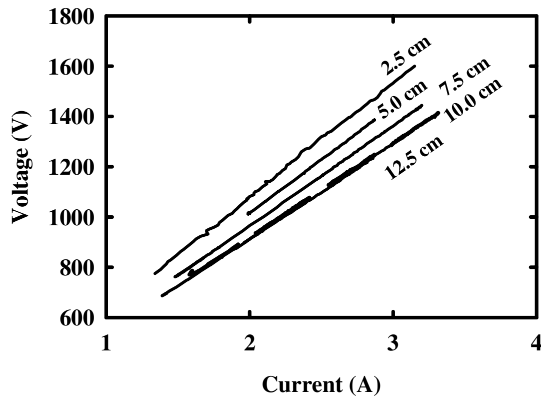

Figure 2. Current–voltage curves for electrodes with varying lengths.

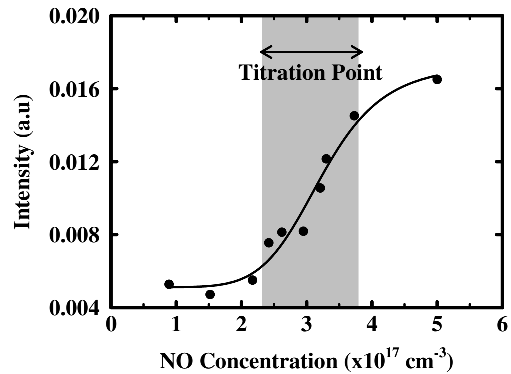

Figure 4. Example of a titration curve for an argon plasma with 6.0 vol% N_2 at 150 W cm^{-3}.

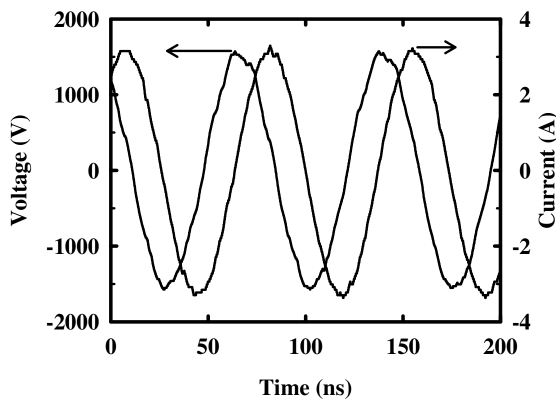

Figure 3. Current and voltage waveforms for an argon discharge with 6.0 vol% N_2 at 150 W cm^{-3}.

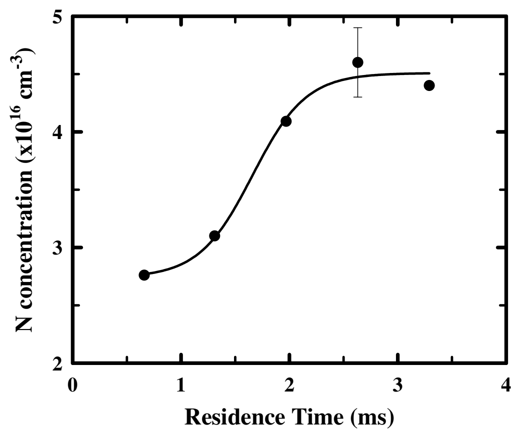

Figure 5. Nitrogen atom density as a function of the residence time.

region, where the voltage increased linearly with the current. The breakdown current was 2.9 A for all the electrodes and the breakdown voltage was nearly constant at 1334 ± 58 V. After ignition, the discharge voltage increased linearly with the current, exhibiting an abnormal glow. It can be seen that all the curves are parallel to each other with the voltage at a given current decreasing with increasing electrode length. Note that the curves for the 10.0 and 12.5 cm electrodes are superimposed on each other.

The root mean square values for the current and voltage waveforms for an argon and 6.0 vol% N_2 plasma are shown in figure 3. The peak values of the current and the voltage are 3.1 A and 1630 V, respectively. Both curves are sinusoidal and the current leads the voltage by 89°. This phase angle indicates that the discharge is capacitive. The 1° phase shift is caused by the resistive nature of the plasma [22]. The current curve does not contain any spikes due to charging and discharging of the quartz. This confirms that this plasma source does not behave like a low frequency DBD [7–11].

3.2. Nitrogen atom density

The ground state nitrogen atom density was determined by titration with nitric oxide [15]. An example of the titration curve obtained with 6.0 vol% nitrogen in argon at 150 W cm^{-3} is shown in figure 4. The titration point is given by the inflection of the curve, which is the shaded region [15]. This method has been compared with three other techniques, including the N_2(B) recombination kinetics, and good agreement was achieved [15].

The N atom concentration as a function of the residence time is presented in figure 5. The plasma conditions were 5.0 L min^{-1} total flow rate, 1.0 vol% N_2, 100 W cm^{-3} and electrode lengths ranging between 2.5 and 12.5 cm. The shortest residence time corresponds to the 2.5 cm electrode, while the longest one to the 12.5 cm electrode. It can be seen that as the residence time increases from 1.3 to 2.0 ms, the N atom density rises from 3.1×10^{16} to 4.1×10^{16} cm^{-3}. Thereafter, the N concentration stays relatively constant. From this data, it was decided that a residence time of 2.6 ms (10.0 cm electrode) would be used in all the other experiments. The per cent dissociation of N_2 under these conditions was 26%.

Shown in figure 6 is the effect of the N_2 feed concentration on the N atom density measured at the exit of the discharge. These experiments were conducted at an argon flow rate of 5.0 L min^{-1} and a power density of 100 W cm^{-3}. It can be seen that the N atom density increased from 4.7×10^{16} cm^{-3} at 1.0 vol% N_2 to 1.2×10^{17} cm^{-3} at 6.0 vol% N_2. Thereafter, the N concentration remained relatively constant. Note that the per cent dissociation decreased from 26% to 12 % as the N_2 feed was raised from 1.0 to 6.0 vol%.

The nitrogen atom concentration was also determined as a function of the applied power. In these experiments, the N_2

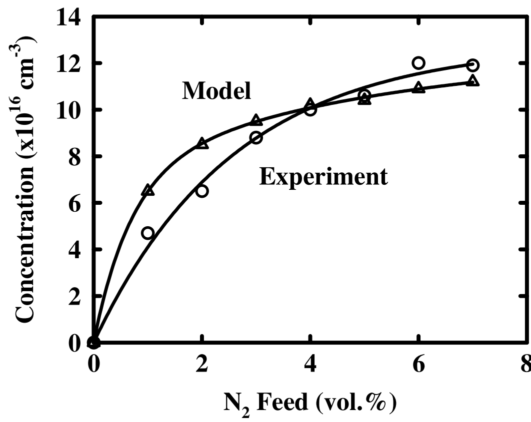

Figure 6. Nitrogen atom concentration as a function of the amount of N_2 fed to the plasma from the experiments and the numerical model.

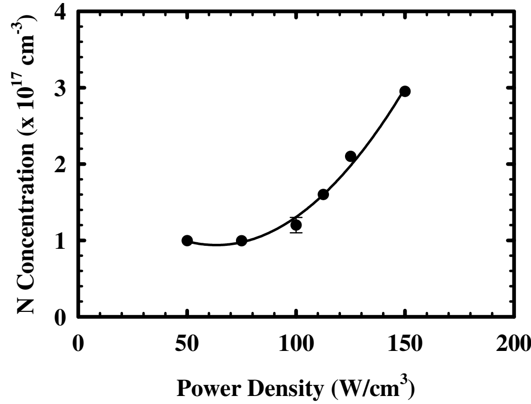

Figure 7. Nitrogen atom concentration as a function of the RF power density.

feed was kept constant at 6.0 vol%. The results are shown in figure 7. Below 100 W cm^{-3}, the N concentration remained constant at 1.0×10^{17} cm^{-3}. Above 100 W cm^{-3}, the N density increased linearly up to 3.0×10^{17} cm^{-3} at 150 W cm^{-3}. The per cent dissociation of the N_2 increased from 12% to 29% over the range of power densities examined. The input power density was not increased higher than 150 W cm^{-3}, to prevent damage to the AE impedance probe, which has a voltage limit of 2.0 kV.

4. Discussion

The plasma density and electron temperature in the discharge were calculated for the different process conditions. First the voltage consumed by the quartz dielectric was estimated using the following formula [23]:

$$V_0 = \varepsilon V, \tag{1}$$

where V is the plasma voltage, V_0 is the applied voltage and ε is the dielectric constant of quartz, equal to 4.2. The sheath thickness, s (m), is obtained by inserting the current density, J (A m^{-2}) and the plasma voltage, V (V), into the following expression [4, 24].

$$J = 1.68\varepsilon_0 \left(\frac{2e\lambda_i}{M}\right)^{1/2} \frac{V^{3/2}}{s^{5/2}}. \tag{2}$$

Here, ε_0 is the permittivity of vacuum (F m^{-1}), e is a unit charge (C), M is the molecular weight of the most abundant rare gas ion, Ar_2^+ (kg mol^{-1}) and λ_i is the mean free path of the ion (m). Equation (2) applies to a collisional sheath model, which is valid at atmospheric pressure. The sheath thickness remained constant at 28 ± 1 μm as the per cent nitrogen to the feed or the power input were varied.

From the sheath thickness, the sheath capacitance can be calculated from

$$C = \frac{1.52\varepsilon_0 A}{s}, \tag{3}$$

where A is the electrode area (m^2). The voltage drop across the sheath is given by

$$V_S = \frac{I}{2\pi f C}, \tag{4}$$

where f is the frequency (Hz). For the plasma operating with 6.0 vol% N_2 at 100 W cm^{-3}, the sheath thickness and its voltage drop are 27 μm and 143 V, respectively. The bulk electric field, E, is then calculated to be 93.5 kV m^{-1}. This yields an E/n value of 7.5×10^{-21} V·m^2, where n is the neutral gas density, 1.3×10^{-25} m^{-3}, at atmospheric pressure.

The plasma density is calculated from the following equation [18, 19, 25]:

$$J = -en_e\mu_e E. \tag{5}$$

Here, μ_e is the electron mobility (V m^{-1} s^{-1}), which is inversely proportional to the pressure, and n_e is the electron density (m^{-3}).

The average electron temperature is calculated from a steady-state power balance on the free electrons in the plasma [18, 26].

$$\varepsilon = n_e \frac{P}{K_B T_g} k_1 I_1 + n_e \left[n_e \langle \sigma_{ei} \upsilon_e \rangle + \frac{P}{K_B T_g} \langle \sigma_{ea} \upsilon_e \rangle \right] \times \frac{2m_e}{M} \frac{3}{2} K_B (T_e - T_g). \tag{6}$$

Here ε is the power density (W m^{-3}), P is the pressure (Pa), T_g is the gas temperature (eV), T_e is the electron temperature (eV), k_1 is the ionization rate coefficient (which is a function of T_e), I_1 is the first ionization energy (eV), $\langle \sigma_{ei} \upsilon_e \rangle$ and $\langle \sigma_{ea} \upsilon_e \rangle$ are the electron–ion and electron–atom collision rate coefficients (which are functions of n_e and T_e). The details of these equations have been published elsewhere [18].

For the argon and nitrogen plasma at 100 W cm^{-3}, the plasma density, electron temperature and the ratio of the electric field to the neutral gas density, E/n remain relatively constant at $3.1 \pm 0.1 \times 10^{12}$ cm^{-3}, 1.27 ± 0.01 eV and $7.5 \pm 0.3 \times 10^{-21}$ V m^2 as the N_2 in the feed varies from 1.0 to 7.0 vol%. However, the electron density in the argon and nitrogen plasma increases from 2.9 to 3.3×10^{12} cm^{-3} as the power density rises from 50 to 150 W cm^{-3}. This occurs because the current density is approximately proportional to the applied power. The electron temperature also increases

Table 1. Reactions and rate constants for the nitrogen plasma.

	Reaction	Rate constant ($cm^3\ s^{-1}$)	Reference
R_1	$e + N_2 \rightarrow 2N + e$	$6.3 \times 10^{-6} T_e^{-1.6} e^{-9.8/T_e}$	[27, 28]
R_2	$e + N_2 \rightarrow N_2^+ + 2e$	$4.7 \times 10^{-13} \sqrt{T_e}(1 + 0.13T_e) e^{-15.7/T_e}$	[29]
R_3	$e + N_2 \rightarrow N^+ + N + 2e$	$4.0 \times 10^{-14} \sqrt{T_e}(1 + 0.08T_e) e^{-25.5/T_e}$	[29]
R_4	$e + N_2 \rightarrow N^* + N + e$	$2.6 \times 10^{-15} \sqrt{T_e}(1 + 0.15T_e) e^{-13.3/T_e}$	[29]
R_5	$e + N_2 \rightarrow N_2(A) + e$	$5.8 \times 10^{-13} \sqrt{T_e}(1 + 0.29T_e) e^{-7.1/T_e}$	[29]
R_6	$e + N^+ \rightarrow N + h\nu$	$1.0 \times 10^{-12} \left(\frac{T_e}{T_g}\right)^{-0.70}$	[29]
R_7	$e + N_2^+ \rightarrow N + N^*$	$2.0 \times 10^{-7} \left(\frac{T_e}{0.03}\right)^{-0.39}$	[29]
R_8	$e + N_3^+ \rightarrow N_2 + N^*$	$3.0 \times 10^{-7} \left(\frac{T_e}{0.03}\right)^{-0.40}$	[29]
R_9	$e + N_4^+ \rightarrow N_2 + N_2(A)$	$6.0 \times 10^{-7} \left(\frac{T_e}{0.03}\right)^{-0.40}$	[29]
R_{10}	$e + Ar \rightarrow Ar^+ + 2e$	$4.0 \times 10^{-12} T_e^{0.5} e^{-15.8/T_e}$	[30]
R_{11}	$e + Ar \rightarrow Ar^* + e$	$1.0 \times 10^{-11} T_e^{0.75} e^{-11.6/T_e}$	[30]
R_{12}	$e + Ar^* \rightarrow Ar^+ + 2e$	$6.8 \times 10^{-9} T_e^{0.67}$	[31]
R_{13}	$e + Ar_2^+ \rightarrow 2Ar^*$	$5.4 \times 10^{-8} T_e^{-0.66}$	[31]
R_{14}	$2e + Ar^+ \rightarrow Ar^* + e$	$5.0 \times 10^{-27} T_e^{-4.5}$ [a]	[32]
R_{15}	$Ar^* + Ar^* \rightarrow Ar^+ + Ar + e$	5.0×10^{-10}	[30]
R_{16}	$Ar^+ + 2Ar \rightarrow Ar_2^+ + Ar$	2.5×10^{-31} [a]	[32]
R_{17}	$N^+ + 2N_2 \rightarrow N_3^+ + N_2$	5.2×10^{-30} [a]	[29]
R_{18}	$N_2^+ + 2N_2 \rightarrow N_4^+ + N_2$	1.9×10^{-29} [a]	[29]
R_{19}	$N^+ + N + M \rightarrow N_2^+ + M$	6.8×10^{-32} [a]	[33, 34]
R_{20}	$N_2^+ + N_2 + M \rightarrow N_4^+ + M$	6.4×10^{-30} [a]	[33, 34]
R_{21}	$N^+ + e + M \rightarrow N + M$	$3.2 \times 10^{-30} T_e^{-1.5}$ [a]	[33, 34]
R_{22}	$Ar^+ + N_2 \rightarrow Ar + N_2^+$	5.0×10^{-10}	[35]
R_{23}	$Ar^* + N_2 \rightarrow Ar + N_2(C)$	3.0×10^{-11}	[36]
R_{24}	$Ar^* + N_2 \rightarrow Ar + N_2(B)$	9.8×10^{-12}	[36]
R_{25}	$Ar^* + N_2 \rightarrow Ar + N + N$	1.6×10^{-11}	[37]
R_{26}	$N + N + M \rightarrow N_2(B) + M$	$8.3 \times 10^{-34} e^{500}/T$ [a]	[17]
R_{27}	$N_2 + N \rightarrow N_2(A) + N$	$1.2 \times 10^{-12} T_e^{-1.5} e^{-6.2/T_e}$	[34]
R_{28}	$N_2(A) + N_2(A) \rightarrow N_2(B) + N_2$	7.0×10^{-11}	[38]
R_{29}	$N_2(A) + N_2(A) \rightarrow N_2(C) + N_2$	3.0×10^{-10}	[39]
R_{30}	$N_2(A) + N_2 \rightarrow N_2 + N_2$	4.0×10^{-17}	[40]
R_{31}	$N_2(A) + N \rightarrow N_2 + N$	9.6×10^{-11}	[40]
R_{32}	$N_2(B) \rightarrow N_2(A) + h\nu$	1.5×10^{5} [b]	[41]
R_{33}	$N_2(B) + Ar \rightarrow N_2(\neq B) + Ar$	8.0×10^{-12}	[42]
R_{34}	$N_2(B) + N_2 \rightarrow N_2(\neq B) + N_2$	3.0×10^{-11}	[43]
R_{35}	$N_2(C) \rightarrow N_2(B) + h\nu$	3.0×10^{7} [b]	[41]
R_{36}	$N_2(C) + N_2 \rightarrow N_2(\neq C) + N_2$	1.0×10^{-10}	[20]

[a] Rate constant is in $cm^6\ s^{-1}$.
[b] Rate constant is in s^{-1}.

from 1.20 to 1.32 eV as the power density rises from 50 to 150 W cm^{-3}. On the other hand, the ratio E/n decreases from approximately 8.0×10^{-21} V m^2 to 7.0×10^{-21} V m^2.

Using the known values of n_e, T_e, T_g and kinetic data obtained from the literature, a model has been developed to predict the concentration profiles in the plasma and the afterglow. A plug–flow model was assumed in which the change in concentration of an individual species with distance is equal to its net rate of consumption (or production) by each of the elementary reactions in the mechanism. The set of coupled first-order differential equations was solved using the commercial software, Polymath. The reaction mechanism is shown in table 1. The units of T_e and T_g are eV and K, respectively. For the different nitrogen feed concentrations at 100 W cm^{-3}, the model predicts a positive ion density of 1.8×10^{12} cm^{-3} in the discharge and an electron density of 3.1×10^{12} cm^{-3}. The plasma may be assumed to be quasineutral within the uncertainty of the rate parameters. In the model, the chemistry is only applied to the bulk of the plasma and not the sheath. This is because the sheath volume is 45 times smaller than the bulk and the density of electrons is much lower in the sheath so that the reaction rates are greatly reduced there.

Shown in the shaded region of figure 8 are the predicted profiles of the reactive species in the plasma with a nitrogen

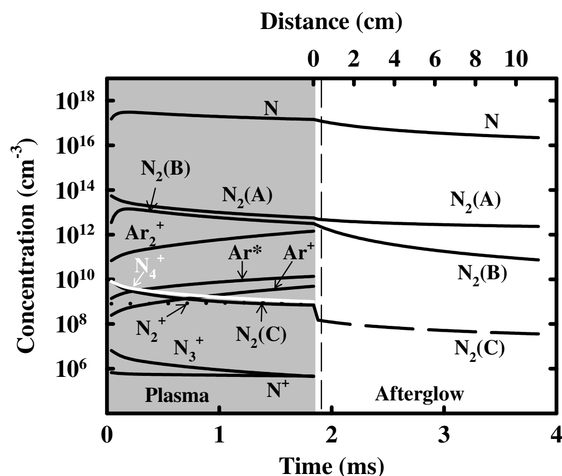

Figure 8. Predicted species concentration profiles in the plasma and afterglow at 6.0 vol% N_2 and 100 W cm^{-3}.

feed concentration of 6.0 vol% and a power density of 100 W cm^{-3}. The end of the plasma is at a distance of 10.2 cm, corresponding to a time of 1.85 ms. At the end of the discharge the concentrations of the neutral species, N, $N_2(A\,^3\Sigma_u)$, $N_2(B\,^3\Pi_g)$, $N_2(C\,^3\Pi_g)$ and Ar*, are 1.4×10^{17}, 5.6×10^{12}, 3.1×10^{12}, 7.0×10^8 and 1.4×10^{10} cm^{-3}, respectively. It can be seen that ground-state N atoms are the most abundant reactive intermediates in the discharge. The concentrations of $N_2(A\,^3\Sigma_u)$ and $N_2(B\,^3\Pi_g)$ are relatively high, $\sim 4.0 \times 10^{12}$ cm^{-3}, because $N_2(A\,^3\Sigma_u)$ is produced through the collision of N_2 with electrons, reaction R_5, while $N_2(B\,^3\Pi_g)$ is produced through N atom recombination, reaction R_{26}. By contrast, the concentration of $N_2(C\,^3\Pi_g)$ is much lower, 7.0×10^8 cm^{-3}, because this species is formed by the recombination of $N_2(A\,^3\Sigma_u)$, reaction R_{29}.

At the end of the discharge the concentrations of the charged species, N^+, N_2^+, N_3^+, N_4^+, Ar^+ and Ar_2^+, are 4.7×10^5, 9.9×10^8, 4.5×10^5, 1.0×10^9, 4.9×10^9 and 1.4×10^{12} cm^{-3}, respectively. The plasma model predicts that Ar_2^+ is more abundant than Ar^+. This is consistent with other studies that have found that at high pressures, the concentration of Ar_2^+ is larger [30, 44, 45]. For example, Petrov *et al* [44] have shown that in an atmospheric pressure the dc argon column, Ar_2^+ constitutes 98% of the total density of all the ions. From the mechanism, it can be seen that the primary pathway for producing N atoms is through electron impact dissociation of the N_2 molecule, R_1. The rate constant for the production of N atoms through N_2 dissociation with Ar*, R_{25}, is two orders of magnitude lower than R_1. Also, the main pathway to consume the N atoms is through three-body recombination, R_{26}.

Reactions R_{26} to R_{36} in table 1 are used to model the afterglow. The other reactions are not used because the density of the electrons and ions decay rapidly beyond the electrode [46]. All the rate constants are calculated at a gas temperature of 250 °C. The concentration profiles in the afterglow as a function of time and distance are shown in figure 8. It can be seen that in the afterglow, the ground state nitrogen atoms are the most abundant reactive intermediates. The dashed line at a distance of 0.5 cm in the afterglow represents the point where the titration experiments were performed. In the case of 100 W cm^{-3} and 6.0 vol% N_2, the N atom density is measured to be $1.2 \pm 0.3 \times 10^{17}$ cm^{-3}, while the model predicts 1.1×10^{17} cm^{-3}, which is excellent agreement.

The numerical simulation was performed for all the different nitrogen feeds into the plasma to see if the model can help explain the observed trend in the N atom density. The values predicted by the simulation at a distance of 0.5 cm downstream of the plasma are compared with the experimental results in figure 6. The trend predicted by the model agrees with that of the experimental data to within the uncertainty of the measurements. The main reaction responsible for the destruction of N atoms is three-body recombination [34]:

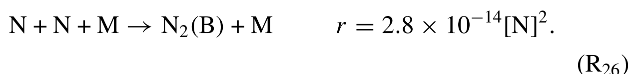

$$\mathrm{N} + \mathrm{N} + \mathrm{M} \rightarrow \mathrm{N_2(B)} + \mathrm{M} \qquad r = 2.8 \times 10^{-14}[\mathrm{N}]^2. \qquad (\mathrm{R}_{26})$$

As the N_2 feed rises from 1.0 to 6.0 vol%, the N atom concentration ([N]) increases from 4.7×10^{16} to 1.2×10^{17} cm^{-3}, and, in turn, the rate of reaction R_{24} increases from 6.3×10^{19} to 4.0×10^{20} cm^3 s^{-1}. The higher rate of recombination limits the production of N atoms.

The plasma source reported herein has several properties that are unique relative to atmospheric pressure discharges reported in the literature [47–50]. The plasma is struck inside a dielectric quartz tube and is driven with radio frequency power at 13.56 MHz. Unlike conventional DBDs operating at 20 to 200 kHz, the time-dependent current curve appears smooth and sinusoidal, without any spikes due to the charging and discharging of the dielectric. Several groups have examined RF DBDs and found that the current waveform does not contain spikes as seen at low frequency [47–49]. Nevertheless, these other groups have demonstrated power densities of only 19.5 W cm^{-3} [47–50]. The atmospheric plasma source described here operates at power densities up to 150 W cm^{-3}, an order of magnitude higher than non-equilibrium discharges published previously.

The relatively high plasma density in the atmospheric pressure discharge, $n_e = 3.1 \times 10^{12}$ cm^{-3}, results in the dissociation of a large fraction of N_2 fed to the source, up to 50%. It is difficult to compare this characteristic with other low temperature atmospheric pressure plasmas, since few authors measure the concentration of reactive species at the exit of the discharge. Lukas and co-workers [51] measured the N atom density in a pure N_2 DBD using laser-induced fluorescence spectroscopy. The plasma source consisted of conical pins that were powered and a grounded plate that was covered with glass, 3.3 mm thick. The spacing between the electrodes was 1.3 mm. They found that the maximum N atom concentration existing inside the filaments ranged from 5.0×10^{14} to 2.0×10^{15} cm^{-3} [51]. The ground-state nitrogen atom density was also measured in a capacitively coupled parallel plate source [15]. No dielectrics were used in this case. It was found that at 1.6 vol% N_2 in He at 100 °C and 15.5 W cm^{-3}, the plasma produced 4.8×10^{15} cm^{-3} N atoms [15, 17]. Increasing the power density to 30.1 W cm^{-3} raised the N atom concentration to a maximum of 1.0×10^{16} cm^{-3}. In the present work, the maximum N atom density recorded at the exit of the discharge was 3.0×10^{17} cm^{-3} at 6.0 vol% N_2 and 150 W cm^{-3}. This is at least 30 times higher than that reported in the previous work.

Acknowledgments

This research was supported in part by a grant from the University of California Discovery program and AMD, and in part by Surfx Technologies LLC. One of the authors, MM, wishes to thank UCLA for a Dissertation Year Fellowship.

References

[1] Kogeschatz U 2004 *Plasma Phys. Control. Fusion* **46** B63
[2] Mazouffre S, Foissac C, Supiot P, Vankan P, Engeln R, Schram D C and Sadehi N 2001 *Plasma Sources Sci. Technol.* **10** 168
[3] Roth J R 1995 *Industrial Plasma Engineering: Principles* (Beograd: Institute of Physics)
[4] Lieberman M A and Lichtenberg A J 1994 *Principles of Plasma Discharges and Material Processing* (New York: Wiley)
[5] Chang J S, Lawless P A and Yamamoto T 1991 *IEEE Trans. Plasma Sci.* **19** 1152
[6] Goldman M and Goldman N 1978 Corona discharges *Gaseous Electronics* vol 1, ed M N Hirsh and H J Oakam (New York: Academic)
[7] Kanazawa S, Kogoma M, Moriwaki T and Okazaki S 1988 *J. Phys. D: Appl. Phys.* **21** 838
[8] Yokoyama T, Kogoma M, Moriwaki T and Okazaki S 1990 *J. Phys. D: Appl. Phys.* **23** 1125
[9] Kogelschatz U 2002 *IEEE Trans. Plasma Sci.* **30** 1400
[10] Radu I, Bartnikas R, Czeremuszkin G and Wertheimer M R 2003 *IEEE Trans. Plasma Sci.* **31** 411
[11] Gherardi N and Massines F 2001 *IEEE Trans. Plasma Sci.* **29** 536
[12] Schoenbach K H, Moselhy M, Shi W and Bentley R 2003 *J. Vac. Sci. Technol.* A **21** 1260
[13] Bardos L and Barankova H 2000 *Surf. Coat. Technol.* **133–134** 522
[14] Schütze A, Jeong J Y, Babayan S E, Park J, Selwyn G S and Hicks R F 1998 *IEEE Trans. Plasma Sci.* **26** 1685
[15] Babayan S E, Ding G and Hicks R F 2001 *Plasma Chem. Plasma Process.* **21** 505
[16] Nowling G R, Babayan S E, Jankovic V and Hicks R F 2002 *Plasma Sources Sci. Technol.* **11** 97
[17] Babayan S E, Ding G, Nowling G R, Yang X and Hicks R F 2002 *Plasma Chem. Plasma Process.* **22** 255
[18] Moravej M, Yang X, Nowling G R, Babayan S E, Chang J P and Hicks R F 2004 *J. Appl. Phys.* **96** 7011
[19] Yang X, Moravej M, Nowling G R, Babayan S E, Penelon J, Chang J P and Hicks R F 2005 *Plasma Sources Sci. Technol.* **14** 314
[20] Simek M and De Benedictis S 1995 *Plasma Chem. Plasma Proc.* **15** 451
[21] Moravej M, Yang X, Penelon J, Babayan S E and Hicks R F 2006 *J. Appl. Phys.* at press
[22] Nilsson J W and Riedel S A 2000 *Electric Circuits* (Englewood Cliffs, NJ: Prentice-Hall)
[23] Young H D 1992 *University Physics* (Reading, MA: Addidon-Wesley)
[24] Lieberman M A 1989 *IEEE Trans. Plasma Sci.* **17** 338
[25] Park J, Henins I, Herrmann H W, Selwyn G S and Hicks R F 2001 *J. Appl. Phys.* **89** 20
[26] Benoy D A, Van der Mullen J A M and Schram D C 1993 *J. Phys. D: Appl. Phys.* **26** 1408
[27] Bultel A, Chéron B G and Vervisch P 1995 *Plasma Sources Sci. Technol.* **4** 597
[28] Cosby P C 1993 *J. Chem. Phys.* **98** 9544
[29] Takaki K, Chang J and Kostov K G 2004 *IEEE Trans. Dielect. Elect. Insul.* **11** 481
[30] Shon J W and Kushner M J 1994 *J. Appl. Phys.* **75** 1883
[31] McCaughey M J and Kushner M J 1991 *J. Appl. Phys.* **69** 6952
[32] Bhoj A N and Kushner M J 2004 *J. Phys. D: Appl. Phys.* **37** 2510
[33] Tatarova E, Dias F M, Gordiets B and Ferreira C M 2005 *Plasma Sources Sci. Technol.* **14** 19
[34] Gordiets B, Ferreira C M, Pinheiro M J and Ricard A 1998 *Plasma Sources Sci. Technol.* **7** 363
[35] Bockel S, Amorim J, Baravian G, Ricard A and Stratil P 1996 *Plasma Sources Sci. Technol.* **5** 567
[36] Loiseau J F, Pignolet P and Held B 1992 *J. Phys. D: Appl. Phys.* **25** 745
[37] Piper L G, Velazco J E and Setser D W 1973 *J. Chem. Phys.* **59** 3323
[38] Nadler I and Rosenwaks S 1985 *J. Chem. Phys.* **83** 3932
[39] Piper L G 1988 *J. Chem. Phys.* **88** 231
[40] Herron J T 1999 *J. Phys. Chem. Ref. Data* **28** 1453
[41] Gilmore F R, Laher R R and Espy P 1992 *J. Phys. Chem. Ref. Data* **21** 1005
[42] Piper L G 1988 *J. Chem. Phys.* **88** 6911
[43] Ionikh Y Z and Chernysheva N V 1990 *Opt. Spectrosc. (USSR)* **68** 598
[44] Petrov G M and Ferriera C M 1999 *Phys. Rev.* E **59** 3571
[45] Pencheva M, Petrov G, Petrova T and Benova E 2004 *Vacuum* **76** 409
[46] Jeong J Y, Babayan S E, Schütze A, Tu V J, Park J, Henins I, Selwyn G S and Hicks R F 1999 *J. Vac. Sci. Technol.* A **17** 2581
[47] Shirafuji T, Kitagawa T, Wakai T and Tachibana K 2003 *Appl. Phys. Lett.* **83** 2309
[48] Moon S Y, Choe W and Kang B K 2004 *Appl. Phys. Lett.* **84** 188
[49] Castro J, Guerra-Mutis M H and Dulce H J 2003 *Plasma Chem. Plasma Process.* **23** 297
[50] Roth J R, Rahel J, Dai X and Sherman D M 2005 *J. Phys. D: Appl. Phys.* **38** 555
[51] Lukas C, Spaan M, Schulz-von der Gathen V, Thomson M, Wegst R, Döbele H F and Neiger M 2001 *Plasma Sources Sci. Technol.* **10** 445